Did You Also Hear That? Spectrum Sensing Using Hermitian Inner Product

Jerry T. Chiang
Advanced Digital Sciences Center
jerry.chiang@adsc.com.sg

Yih-Chun Hu
University of Illinois at Urbana–Champaign
yihchun@illinois.edu

***Abstract*—Spectrum sensing is one of the most important enabling techniques on which to build a cognitive radio network. However, previously proposed techniques often have shortcomings in non-ideal environments: 1) An energy detector is simple but cannot perform in face of uncertain noise power; 2) A matched filter is the optimal detector, but performs poorly with clock drifts; 3) Eigenvalue-based blind feature detectors show great promise, but cannot detect signals that are noise-like; and 4) Above protocols all rely on field survey to determine the proper decision thresholds.**

We propose HIPSS and its extension Δ-HIPSS that are based on the Hermitian-inner-product of two observations acquired by a wireless receiver over multiple radio paths. HIPSS and Δ-HIPSS are lightweight and through extensive analysis and evaluation, we show that 1) HIPSS and Δ-HIPSS are robust in the presence of noise power uncertainties; 2) HIPSS and Δ-HIPSS require neither a much longer observation duration nor complex computation compared to an energy detector in ideal setting; 3) HIPSS and Δ-HIPSS can detect noise-like primary signals; and 4) Δ-HIPSS can reliably return sensing decisions without necessitating any field surveys.

I. Introduction

With the proliferation of wireless technology, the wireless frequency spectrum has become a scarce and heavily contended resource. Service providers spend billions of dollars every year in securing their exclusive rights to a portion of the spectrum. However, previous measurement data shows that most of the spectrum is underutilized; for example, even the heavily-used 850 MHz cellular band is only 50% occupied in the Chicago metropolitan area [1].

Mitola, III and Mcguire, Jr. proposed the concept of *cognitive radio*: a radio that, without exclusive rights to a frequency band, can opportunistically use the frequency band when it is unoccupied [2]. A spectrum sensing technique enables a cognitive radio to determine whether a particular frequency band is occupied, so that the cognitive radio can subsequently determine whether it could emit power on that spectrum without interfering the primary transmitter.

This study is partially supported by the research grant for the Human Sixth Sense Program at the Advanced Digital Sciences Center from Singapore's Agency for Science, Technology and Research (A*STAR). This material is also based upon work partially supported by NSF under Contract No. NSF CNS-0953600. The views and conclusions contained here are those of the authors and should not be interpreted as necessarily representing the official policies or endorsements, either express or implied, of the NSF, the University of Illinois, the Advanced Digital Sciences Center, the U.S. Government or any of its agencies, or the Singapore Government or any of its agencies.

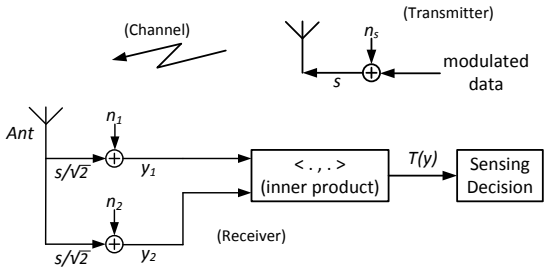

Fig. 1: Block diagram of a transmitter and a HIPSS detector

In this paper, we propose *HIPSS*, Hermitian-Inner-Product-based Spectrum Sensing, a simple but powerful spectrum sensing technique that can distinguish signals of unknown characteristics (even noise-like signals) from circuit noises. We illustrate the HIPSS detector in Fig. 1. HIPSS exploits the assumptions that circuit noise dominates other noise sources and physically separated RF circuits produce independent noises. HIPSS is a *blind spectrum sensing method*: it seeks to determine whether there is a signal in the channel without knowing in advance any signal characteristic. The concept of HIPSS is easy to understand: if two people who trust each other hear the same sound, they would be convinced that the sound is real. We also present an extension Δ-*HIPSS* that learns the field parameters on-the-fly, and does not require any preliminary field surveys.

In this paper, we show that:

1) HIPSS is able to outperform energy detectors or feature detectors by robustly detecting primary signals even when the noise distribution is changing or when the signal feature is not conspicuous (e.g. noise-like signals).
2) With a small penalty in performance; Δ-HIPSS removes any necessity for preliminary field surveys, making Δ-HIPSS a promising sensing technique for sensor networks, so that sensors can sleep without having to recalibrate after waking up.

We evaluate HIPSS by first showing that noise samples from different RF circuits (on a single Universal Software Radio Platform, USRP) are mostly uncorrelated, thus noise observations are almost orthogonal. We then plot the receiver operating characteristic (ROC) of HIPSS compared with an energy detector and a blind feature detector in real-life experiments. We also use extensive Monte Carlo simulation to

978-1-4673-5946-7/13/$31.00 ©2013 IEEE

demonstrate how HIPSS and Δ-HIPSS can outperform the energy and blind feature detectors.

II. Related Work

Spectrum sensing is an important enabling primitive for cognitive radio networks. Copious sensing techniques exist in the literature and can generally be categorized into three classes [3]: 1) matched filtering, 2) energy detection, and 3) feature detection.

In the matched filtering detection scheme, the receiver passes a received signal through a matched filter, which is known to filter out as much noise as possible without impacting the signal [4], which in turn minimizes the bit-error probability in a demodulation system. However, a matched filtering scheme requires receivers to have extensive prior knowledge of the primary user's transmission circuit.

In the energy detection schemes, the receiver measures the energy of the received signal (inclusive of noise) in a particular frequency band, and decides there is a signal if the energy exceeds a threshold [5], [6], [7]. Cabric et al. studied sensing techniques based on matched filtering a pilot tone versus energy detection, and derived the number of necessary samples, when the signal-to-noise ratio (SNR) is given, to satisfy a pair of desired probability of detection and probability of false alarm [6]. Cabric et al. found that the number of necessary samples in matched filtering and energy detection schemes are $O(\text{SNR}^{-1})$ and $O(\text{SNR}^{-2})$, respectively. The authors noted that matched-filter-based detection suffers from drifts and offsets of the local oscillators, and energy detection suffers from uncertainty in noise power.

Feature detection schemes exploit the built-in structures of the transmitted signals. For example, if a transmitter periodically transmits a beacon, a receiver can autocorrelate the received signal to find the periodicity and decide that the frequency band is occupied when a distinct periodicity exists [8]; this type of schemes is commonly known as *cyclostationarity-based sensing*.

HIPSS seeks to identify both structured transmissions as well as noise-like signals. Under this setting, cyclostationarity-based sensing is not applicable, and feature extraction becomes a difficult blind classification problem. For example, Zeng and Liang propose finding the eigenvalues of the covariance matrix of the sampled signal, and then if the maximum eigenvalue of the covariance matrix is much larger in value than the minimum eigenvalue, the receiver can detect the signal [9]. The maxi-min eigenvalue (MME) method is a detector based on how strong the strongest signal pattern is compared to the noise. We can expect that as the pattern diminishes in the low SNR regime, or *when the signal is noise-like*, the signal pattern becomes drowned out, the eigenvalues are clustered together, and detection becomes difficult. Indeed, Zeng and Liang simulated the MME method and found that the eigenvalue-based method misses detection much more often than an energy detector with constant noise variance when the SNR drops below a certain level.

Several prior studies propose using the diversity gain of a multiple-input-multiple-output (MIMO) system to achieve better performance; that is, these methods seek to accent the signals by *summing* over possibly weighted observations [10], [11]. HIPSS is novel in moving away from the MIMO decoding ideology and using the *inner product* between observations as a detection statistic.

Sharma and Wallace propose using the maximum cross-correlation of the observations from multiple sensors as the test statistic [12]. Oude Alink et al. recently also described using cross correlation between observations as the test statistic [13] and showed that phase difference between observations leads to an SNR wall. Our paper builds a deeper understanding through extensive evaluation, and more importantly proposes an improvement that eliminates the necessity in field surveys.

III. System Model and Assumptions

In this paper, we assume that the transmitted signal is memoryless and we do not have any prior knowledge of the transmitted signal. Our assumption takes away any possibility of using matched filtering or non-blind feature detection schemes for sensing purposes. The upside to this assumption is that our proposed methods can be used to detect noise-like signals as well as structured signals.

We assume that the transmitted signal is independent from noise. Our analysis assumes zero phase offset between observations. This assumption is reasonable since, unlike noise uncertainties or clock drifts, the phase offset between observations in HIPSS is due to path difference and is constant, thus the receiver can easily compensate for this offset (as shown by the success of synchronous MIMO).

IV. The HIPSS Method

A. Intuition

HIPSS uses the Hermitian-inner-product between two observations as the test statistic. If either observation is noise-free, and the two observations have no phase offset, then their inner product corresponds to the peak of the output of a matched filter. In other words, without any prior knowledge of the primary signal, HIPSS tries to produce the maximum output of a matched filter by *using one observation (half the received signal) to filter the other*.

Because both observations are corrupted by noise, we show in Section V that for HIPSS, the required number of samples to satisfy a given pair of detection and false alarm probabilities is more similar to an energy detector rather than a matched filter detector. However, we also show that the mimicry of a matched filter without requiring prior information uniquely makes HIPSS robust in the presence of unstructured, noise-like signal and noise with non-constant power.

B. Definitions

In order to quantitatively discuss and analyze HIPSS, we first define the following symbols and terms. We define a *sample* to be one amplitude (voltage) reading at an analog-to-digital converter (ADC). Since the power of the incoming

signal is split between two paths, each sample is $1/\sqrt{2}$ times the amplitude of the incoming signal. We then define an *observation* to be a collection of samples taken over time at one ADC; and a *tuple* to be a collection of samples taken across ADCs at one time instance.

As shown in Fig. 1, let the received signal be $y_1[k] = s[k]/\sqrt{2} + n_1[k]$ and $y_2[k] = s[k]/\sqrt{2} + n_2[k]$, respectively at the first ADC and the second ADC. We refer to n_i as noise, and assume that n_i has zero mean and is additive, white, and (circular-symmetric) complex-Gaussian distributed with variance σ_i^2 for $i \in \{1, 2\}$. We also assume that n_1 and n_2 are independent, this assumption can be justified by observing that the correlated portion of the noise observations is indistinguishable from the unknown signal.

Define a *test statistic* $T(y)$ to be the real part of the Hermitian inner product of the two observations divided by K, which is the number of samples per observation:

$$\begin{aligned} T(y) &= \frac{1}{K}\mathfrak{Re}\left\{\langle y_1, y_2\rangle\right\} \\ &= \frac{1}{K}\mathfrak{Re}\left\{\frac{1}{2}\langle s, s\rangle + \frac{1}{\sqrt{2}}\langle s, n_1 + n_2\rangle + \langle n_1, n_2\rangle\right\}. \end{aligned}$$

A *detection strategy* is a function $F : \mathbb{R}^{2K} \to \{0, 1\}$, where F maps the $2K$ samples (K from each observation) to a binary decision. We follow the convention and define:

1) The *probability of false alarm* P_{FA} is the probability of F returning 1 when $s = 0$; and
2) The *probability of missed detection* P_{MD} is the probability of F returning 0 when $s \neq 0$. The *probability of detection* P_D is the complement of P_{MD}.

The *receiver operating characteristic* (ROC) of a detection strategy is the curve of detection probability versus the false alarm probability.

Finally, we define the *signal power* to be $P = \frac{1}{K}\langle s, s\rangle$.

C. Details of the HIPSS Method

We propose the HIPSS method in the form of a hypothesis test. Let

$$\begin{aligned} &\mathcal{H}_0 : s = 0, \langle y_1, y_2\rangle = \langle n_1, n_2\rangle \\ &\mathcal{H}_1 : s \neq 0, \langle y_1, y_2\rangle = \langle s/\sqrt{2} + n_1, s/\sqrt{2} + n_2\rangle, \end{aligned}$$

and let Γ be the threshold above which the detection strategy returns 1[1]. We can then rewrite the error probabilities as

$$\begin{aligned} P_{FA}(\Gamma) &= \mathbf{Pr}\left(T(y) > \Gamma | \mathcal{H}_0\right) \\ P_{MD}(\Gamma) &= \mathbf{Pr}\left(T(y) \leq \Gamma | \mathcal{H}_1\right) = 1 - P_D. \end{aligned}$$

The threshold Γ is chosen to optimize the balance between the false alarm and the detection probabilities.

[1]We show later in the section that the variance of $T(y)|\mathcal{H}_1$ is greater than that of $T(y)|\mathcal{H}_0$, thus the detection strategy, when given a large negative test statistic, should return 1 and not 0. However, with a large number of samples per observation, the difference in means is overwhelming against the variance, and using the suboptimal detection strategy only incurs negligibly higher error probabilities.

To analyze HIPSS in later sections, we first derive some properties of the test statistic $T(y)$. Since s is deterministic from the detector's perspective, and each n_i is independent identically distributed (i.i.d.) over samples, the central limit theorem dictates that the test statistic $T(y)$ converges in distribution. We first observe that after expansion, each term of $T(y)$ is approximately normally distributed:

$$\begin{aligned} \frac{1}{K}\mathfrak{Re}\left\{\langle s, n_1 + n_2\rangle\right\} &= \frac{1}{K}\sum_{k=1}^{K}\mathfrak{Re}\left\{s\right\}\mathfrak{Re}\left\{n_1 + n_2\right\} + \\ &\qquad \frac{1}{K}\sum_{k=1}^{K}\mathfrak{Im}\left\{s\right\}\mathfrak{Im}\left\{n_1 + n_2\right\} \\ &\sim \mathcal{N}\left(0, \frac{\langle s, s\rangle}{K}\frac{\sigma_1^2 + \sigma_2^2}{2K}\right), \\ \frac{1}{K}\mathfrak{Re}\left\{\langle n_1, n_2\rangle\right\} &\sim \mathcal{N}\left(\mu_{nn}, \sigma_{nn}^2\right), \end{aligned}$$

where

$$\begin{aligned} \mu_{nn} &= \frac{1}{K}\mathrm{E}\left[\mathfrak{Re}\left\{\langle n_1, n_2\rangle\right\}\right] \\ &= \frac{1}{K}\mathrm{E}\left[\mathfrak{Re}\left\{n_1\right\}\mathfrak{Re}\left\{n_2\right\} + \mathfrak{Im}\left\{n_1\right\}\mathfrak{Im}\left\{n_2\right\}\right] = 0, \end{aligned}$$

$$\begin{aligned} \sigma_{nn}^2 &= \frac{1}{K^2}\mathrm{var}\left(\mathfrak{Re}\left\{\langle n_1, n_2\rangle\right\}\right) \\ &= \frac{2}{K}\mathrm{E}\left[\left(\mathfrak{Re}\left\{n_1\right\}\mathfrak{Re}\left\{n_2\right\}\right)^2\right] \qquad \text{(by symmetry)} \\ &= \frac{2}{K}\mathrm{E}\left[\mathfrak{Re}\left\{n_1\right\}^2\right]\mathrm{E}\left[\mathfrak{Re}\left\{n_2\right\}^2\right] \qquad \text{(i.i.d.)} \\ &= \frac{\sigma_1^2\sigma_2^2}{2K}. \end{aligned}$$

We then combine the three terms,

$$\begin{aligned} T(y) &\sim \mathcal{N}\left(\mu_T, \sigma_T^2\right), \\ \mu_T &= \frac{\langle s, s\rangle}{2K} = \frac{P}{2} \\ \sigma_T^2 &= \frac{\langle s, s\rangle\left(\sigma_1^2 + \sigma_2^2\right)}{4K^2} + \frac{\left(\sigma_1^2\sigma_2^2\right)}{2K} \\ &= \frac{1}{2K}\left(\frac{P}{2}(\sigma_1^2 + \sigma_2^2) + (\sigma_1^2\sigma_2^2)\right). \end{aligned}$$

If no signal is present, that is if $s = 0$, then

$$T(y)|\mathcal{H}_0 \sim \mathcal{N}\left(0, \frac{\sigma_1^2\sigma_2^2}{2K}\right)$$

is simply a zero-mean Gaussian variable that converges to 0 as K goes to infinity.

D. Avoiding the Field Survey Phase: Δ-HIPSS

It is intuitive to see that the false alarm probability only depends on the number of samples per observation and the product of noise variances, $\sigma_1^2\sigma_2^2$ (since by definition, P_{FA} is determined when no signal is present). Thus if we can upper bound the product of noise variances, we can upper bound the false alarm probability, and derive a corresponding lower bound on the detection probability for any given SNR.

To the best of the authors' knowledge, all prior spectrum sensing schemes burden the secondary user with a field survey phase, during which the user learns the best threshold. For example, an energy detector must use the survey phase to learn the noise level; and future noise level that deviates from that learned during the survey degrades the sensing performance.

We extend the concept of HIPSS by realizing that the two observations can enable the detector to estimate, in real time, an upper bound on the product of noise variances ($\sigma_1^2\sigma_2^2$):

$$\begin{aligned}\frac{1}{K}\langle y_1 - y_2, y_1 - y_2\rangle &= \frac{1}{K}\langle n_1 - n_2, n_1 - n_2\rangle \\ &\approx 2\mathrm{E}\left[\mathfrak{Re}\left\{n_1\right\}^2 + \mathfrak{Re}\left\{n_2\right\}^2\right] \\ &= \sigma_1^2 + \sigma_2^2 \\ \text{(with high prob.)} \;\Rightarrow \left(\sigma_1^2\sigma_2^2\right) &\leq \frac{\left(\langle y_1 - y_2, y_1 - y_2\rangle\right)^2}{4K^2}.\end{aligned}$$

This upper bound may be loose if the two observations have significantly different SNRs. However, in a realistic setting, by using two RF paths that are close in proximity (hence impacted by similar fading parameters and similar noise temperatures) and each built using the same components, the observed SNRs should not be significantly different.

Thus, the receiver has a pretty good knowledge on the distribution of $T(y)|\mathcal{H}_0$. When $T(y)$ is far[2] from the theoretical mean 0, detection is possible even without perfect knowledge of the noise variance. This is a very attractive feature especially for sensor networks: the sensors do not have to recalibrate after sleeping.

Let $\sigma_{nn}^{*^2} = \frac{\left(\langle y_1 - y_2, y_1 - y_2\rangle\right)^2}{(4K^2)(2K)} \approx \left(\frac{\sigma_1^2 + \sigma_2^2}{\sqrt{8K}}\right)^2$. Let the desired (nominal) false alarm probability be P_{FA}^*, and the threshold be $\Gamma^* = \sigma_{nn}^* Q^{-1}\left(P_{FA}^*\right)$, then the detection strategy

$$F\left(T(y)\right) = \begin{cases} 0 & \text{if } T(y) < \Gamma^* \\ 1 & \text{if } T(y) \geq \Gamma^* \end{cases}$$

results in detection probability

$$P_D(\Gamma^*) \geq Q\left(\frac{\Gamma^* - P/2}{\sqrt{\frac{P}{\sqrt{2K}}\sigma_{nn}^* + \sigma_{nn}^{*^2}}}\right) \quad \text{(with high prob.)}.$$

V. Analysis: Error Probability and Required Number of Samples

With the derived distribution of the test statistic $T(y)$, it is clear that

$$\begin{aligned}P_{FA}(\Gamma) &= Q\left(\frac{\Gamma}{\sqrt{\sigma_1^2\sigma_2^2/2K}}\right) \\ P_D(\Gamma) &= Q\left(\frac{\Gamma - \frac{P}{2}}{\sqrt{\frac{1}{2K}\left(\frac{P}{2}(\sigma_1^2 + \sigma_2^2) + (\sigma_1^2\sigma_2^2)\right)}}\right),\end{aligned}$$

[2]For example, away by five maximum standard deviations.

where $Q(\cdot)$ is the tail-probability Q-function. As in the analysis by Cabric et al., we can manipulate the above equations to obtain K in terms of P_{FA} and $P_D = 1 - P_{MD}$ [6]:

$$\begin{aligned}\Gamma &= \sqrt{\frac{\sigma_1^2\sigma_2^2}{2K}}Q^{-1}\left(P_{FA}\right) \\ &= \sqrt{\frac{1}{2K}\left(\frac{P}{2}(\sigma_1^2 + \sigma_2^2) + (\sigma_1^2\sigma_2^2)\right)}Q^{-1}(P_D) + \frac{P}{2}\end{aligned}$$

If we assume that the two RF paths suffer from the same amount of noise power, i.e. $\sigma_1 = \sigma_2 = \sigma$, then define the signal to noise ratio as $\mathrm{SNR} = P/\sigma^2$; then by manipulating the above equation, we obtain

$$K = 2\left(\frac{Q^{-1}\left(P_{FA}\right) - \sqrt{1 + \mathrm{SNR}}Q^{-1}\left(P_D\right)}{\mathrm{SNR}}\right)^2$$

This analysis shows that HIPSS operates more similar to an energy detector than a matched filter since $K' = O\left(\mathrm{SNR}^{-1}\right)$ in a matched filter detector [6]. Moreover, the required number of samples for HIPSS to satisfy a given detection and false alarm probabilities is roughly twice of that for an energy detector. This is intuitive because by splitting the signal into two, the SNR of each path is half of the original SNR, hence the total number of samples of HIPSS is four times (equivalently, twice for each path) of that of an energy detector!

The advantage of HIPSS and Δ-HIPSS over an energy detector is not in the number of samples, but their robustness. We show in Section IV that, for both HIPSS and Δ-HIPSS,

$$\begin{aligned}\lim_{K\to\infty} \mathrm{E}\left[T(y)|\mathcal{H}_0\right] &= 0 \\ \lim_{K\to\infty} \mathrm{E}\left[T(y)|\mathcal{H}_1\right] &= P/2 > 0\end{aligned}$$

when the noise samples are independent. Thus, the expected value of $T(y)|\mathcal{H}_0$ does not equal the expected value of $T(y)|\mathcal{H}_1$. Moreover, the variance of the test statistics decreases as the number of samples increases, even if there exists uncertainty in the noise variances. Thus, unlike an energy detector, neither HIPSS nor Δ-HIPSS experience an SNR-wall when the noise power is uncertain or varying.

VI. Evaluation

In this section, we use the Universal Software Radio Platform (USRP) to

1) empirically test the assumptions made in Section V that n_1 and n_2 are independent; and
2) detect an artificially generated signal at 902 MHz and show the receiver operating characteristic (ROC) of a HIPSS detector.

A. Correlation of Observations

We use a first generation Universal Software Radio Platform (USRP1), equipped with one FLEX900 800 MHz–1000 MHz transceiving daughterboard and one DBS-Rx 800 MHz–2400 MHz receiving daughterboard; the USRP1 is

MIMO-capable when equipped with two transceiving daughterboards. Since our USRP1 setup contains two receivers, we can use it as a receiving system with multiple ADCs. We perform the experiments in this subsection at the 903 MHz band. We show the spectrum density of the noise in Fig. 2a.

We first tune the center frequencies of both daughterboards to 903.001 MHz with gain of 30, and program each daughterboard to collect 12,000 samples at 500,000 samples per second (500 ksps), the daughterboards are triggered by a common clock on the USRP1, but each daughterboard has its own phase lock loop (PLL). We use a rat-race RF hybrid coupler that divides the incoming signal into two, and connect each output of the hybrid to a USRP daughterboard.

After obtaining the observations, we pair the observations together so that each data tuple represents four samples, two from each daughterboard (in-phase and quadrature). We calculate the real part of the complex correlation coefficient of the two observations and present the histogram in Fig. 2b. We observe that the correlation coefficient between observations ranges from -0.1 to 0.1, indicating that noise observations are mostly uncorrelated. Our formulation absorbs the correlated portion into the signal, thus this small correlation increases the false alarm probability; Section VIII-B explores this issue in more detail.

We show the normal QQ-plots of the four observations in Fig. 2c to 2f. The high linearity of the data points indicate that the noise observations are very close to normally-distributed.

Finally, to show the probability density, we process these 12,000 data tuples using a two-dimensional kernel density estimator (2D-KDE)[3]. In KDE, each data observation is transformed into a normal density function, and the resulting density is the aggregate of these individual functions. KDE is similar to a histogram, but the output is smoother. Fig. 2g to 2l shows the contour plots of the estimated density from observations. Since the QQ plots show that the observations are normally distributed, the concentric-circular contours verifies that the noises are almost independent between observations (both in-phase versus quadrature and ADC versus ADC).

We then connect an antenna to a Windfreak SynthUSB signal generator[4] to emit a persistent 903 MHz sinusoidal signal over air. Fig. 3a shows the spectrum density. We again derive the correlation coefficient of the two observations and present the histogram in Fig. 3b. We observe that the correlation coefficient between observations are heavily weighted toward +1 and -1, indicating that observations of the same signal are highly correlated. We observe negative correlations possibly because the PLLs are stuck in different phases.

Again, we use KDE to estimate the distribution and plot the contours in Fig. 3c to 3h. The observed distribution forms an ellipse on the plane, corresponding to plotting a sinusoid versus a delayed version of itself. In particular, when plotting the in-phase (quadrature) readings versus each other, the resulting figure shows an almost-straight line, showing a high degree of correlation between the two readings. When plotting other combinations of quadrature reading versus in-phase reading, the foci are located either on the x-axis or the y-axis, indicating that the two readings are 90 degrees out-of-phase. The difference in daughterboard gains is reflected in the eccentricity of the ellipses in Fig. 3e and 3f.

[3]Source code at http://www.maths.lth.se/matstat/wafo/download

[4]http://www.windfreaktech.com/synthusb.html

B. ROC Obtained by USRP

In this section, we compare three sensing methods: 1) HIPSS, 2) energy detector, and 3) the MME feature detector by Zeng and Liang [9]. We use an HP E4433B signal generator as the transmission source. We set the frequency of the signal generator at 902.001 MHz with various amplitude settings. We also perform our experiment by using both a sinusoidal output and an AWGN output. We use a rat-race RF hybrid coupler that divides the output signal into two, and connect each output of the hybrid to a USRP daughterboard. We set the gain of the USRP daughterboards to 50, and obtain 100 different test statistics ($T(y)|\mathcal{H}_1$) each derived from two 12,000-sample observations. For signal consistency, we let the energy and MME detectors sum the two observations before deriving, respectively, the signal energy and the covariance eigenvalue. Only the in-phase portion of the signal is used for this experiment.

Since the PLLs cause the inner product to at times be negative, we deviate slightly from our protocol and use the absolute value of the inner product as our test statistic. For obtaining the test statistic of the MME method, we use the parameters in the original paper: $M = 4$, $P = 2$, $L = 8$.

We then similarly obtain another 100 different test statistics by powering off the RF output of the signal generator. We vary Γ so as to obtain the false alarm and the corresponding detection probabilities.

Fig. 4 plots our experimental results. In Fig. 4c and 4f, we see that when the signal power is low, all three methods suffer and the ROC's are not (much) better than guessing. In Fig. 4b, we observe that when the signal has an underlying structure (e.g. sinusoidal), the MME detector can outperform HIPSS. However, Fig. 4e shows that when the signal is noise-like, the MME detector does not perform much better than guessing.

All plots of Fig. 4 show that HIPSS can provide similar detection capability as an energy detector. One anomalous result is the performance of the MME detector in Fig. 4d. We suspect that the 902 MHz frequency band may contain some low-power signal, so that the supposedly noise-only data appears to have more structure than the AWGN-signal data, resulting in high false-alarm probability. Additionally, all methods perform better with sinusoidal signal than with noise-like signal. One possible cause is the difficulty for the PLLs to correctly lock onto the noise-like signals.

VII. Octave Simulation

In this section, we validate our theoretical derivation using Monte Carlo simulation on GNU Octave, which allows us to much better control the noise characteristics. We let s be a signal such that $||s||^2 = 1$, and let $\sigma^2 = \sigma_1^2 = \sigma_2^2 = (\text{SNR})^{-1}$

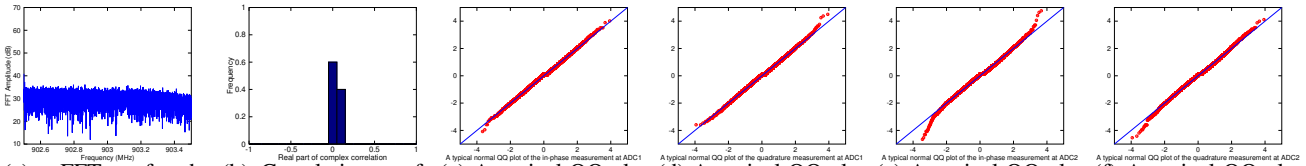

(a) FFT of the spectrum around 903 MHz, noise-only (b) Correlation coefficient of the observations (c) A typical QQ plot of I_1, assuming normal distribution (d) A typical QQ plot of Q_1, assuming normal distribution (e) A typical QQ plot of I_2, assuming normal distribution (f) A typical QQ plot of Q_2, assuming normal distribution

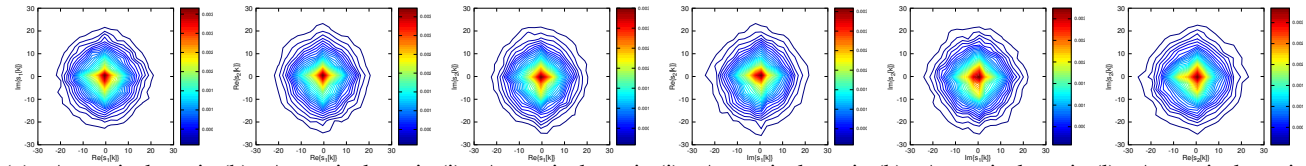

(g) A typical estimated contour using KDE, I_1 versus Q_1 (h) A typical estimated contour using KDE, I_1 versus I_2 (i) A typical estimated contour using KDE, I_1 versus Q_2 (j) A typical estimated contour using KDE, Q_1 versus I_2 (k) A typical estimated contour using KDE, Q_1 versus Q_2 (l) A typical estimated contour using KDE,I_2 versus Q_2

Fig. 2: With only noise at the 903 MHz band, this figure shows the correlation coefficient and normality of the observations, as well as the spectrum density and distribution of measured tuples. Only for this plot, I_k (Q_k) indicates the in-phase (quadrature) reading acquired from the k^{th} ADC.

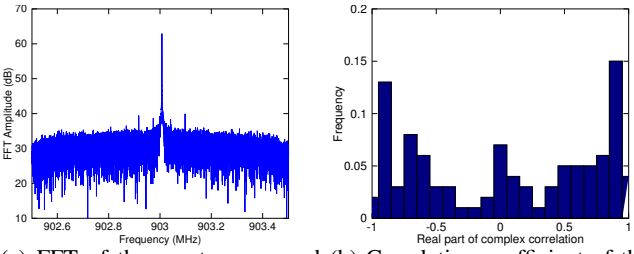

(a) FFT of the spectrum around 902 MHz, with sinusoidal signal observations (b) Correlation coefficient of the observations

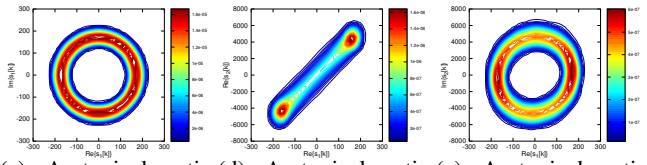

(c) A typical estimated contour using KDE, I_1 versus Q_1 (d) A typical estimated contour using KDE, I_1 versus I_2 (e) A typical estimated contour using KDE, I_1 versus Q_2

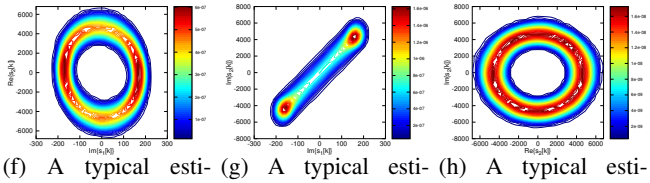

(f) A typical estimated contour using KDE, Q_1 versus I_2 (g) A typical estimated contour using KDE, Q_1 versus Q_2 (h) A typical estimated contour using KDE, I_2 versus Q_2

Fig. 3: With a persistent 903 MHz sinusoidal signal, this figure shows the correlation coefficient of the observations, as well as the spectrum density and distribution of measured tuples.

except in the last part of this section. For our Octave simulations, we assume that noises are independent over samples and ADCs, and assume zero phase offset between the two RF paths.

This section is divided into three parts:

1) We show the ROCs of HIPSS and Δ-HIPSS in the presence of noise power uncertainties;
2) We show the relationship between the probability of detection and length of observations; and
3) We show the relationship between the probability of detection and the signal-to-noise ratio (SNR).

A. *ROCs of HIPSS and Δ-HIPSS*

We examine the robustness of HIPSS and Δ-HIPSS in this section. In particular, we present the ROCs of HIPSS and Δ-HIPSS by plotting the detection probability versus the false alarm probability (for Δ-HIPSS, we use the nominal false alarm probability). The ROC of a robust detection method must lie outside the box defined by $(0.5 \leq P_{FA} \leq 1, 0 \leq P_D \leq 0.5)$, i.e. the lower-right quadrant of the plot.

We perform Monte Carlo simulations to compare four detection techniques: 1) HIPSS, 2) energy detector, 3) the MME feature-detection method, and 4) the Δ-HIPSS extension. In each round, we simulate 16,000 samples and derive the test statistic associated with each of the four schemes. These test statistics enable us to derive the detection probability versus the false alarm probability for each of the four schemes. For the first three schemes, we assume the receiver has perfect knowledge of the expected noise power; but we assume the Δ-HIPSS receiver has zero prior knowledge of the noise power.

We let the nominal SNR be -20 dB, and consider three different noise uncertainties: 0 dB, 0.8 dB, and 1.5 dB. We also consider two different signal structures: a quadrature sinusoidal signal (the in-phase and quadrature portions are each a sinusoid), and a quadrature noise-like signal (such that the in-phase and quadrature portions are together complex normally distributed with variance 0.01 times that of the noise). We obtain 300 sets of test statistics for each parameter combination. For simulating the MME detector [9], we use the same parameters as those in the original paper: $M = 4, P = 2, L = 8$.

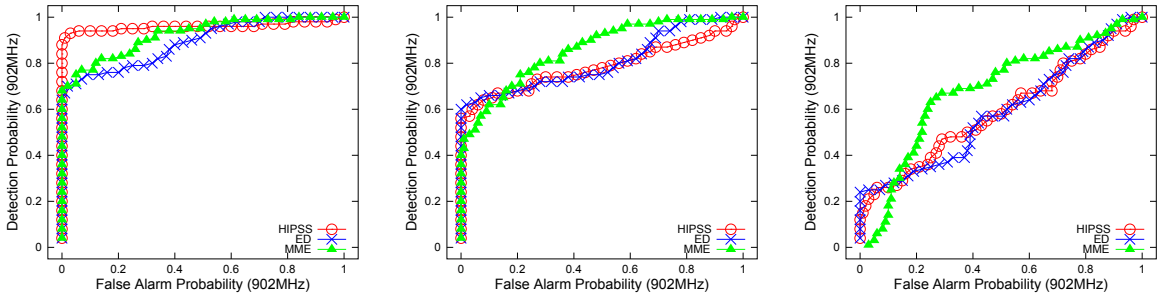

(a) Center frequency = 902 MHz, sinusoidal signal with power = -85 dBm (b) Center frequency = 902 MHz, sinusoidal signal with power = -90 dBm (c) Center frequency = 902 MHz, sinusoidal signal with power = -95 dBm

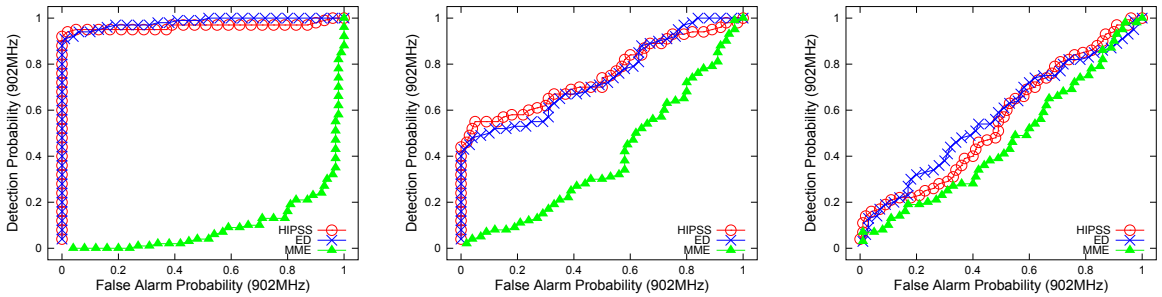

(d) Center frequency = 902 MHz, AWGN signal with power = -75 dBm (e) Center frequency = 902 MHz, AWGN signal with power = -85 dBm (f) Center frequency = 902 MHz, AWGN signal with power = -95 dBm

Fig. 4: ROC's (detection probability versus false alarm probability) of HIPSS, sum-based energy-detector, and MME detector with either sinusoidal or AWGN signal at 902 MHz with various signal powers. Data collected using USRP.

Fig. 5 shows our simulation results. We observe that when there is no noise uncertainty, the energy detector outperforms HIPSS and Δ-HIPSS. However, with 1.5 dB of uncertainty in noise power, the performance of the energy detector deteriorates substantially.

The MME feature detector performs quite well when the signal is sinusoidal, but its performance is significantly reduced when the signal is noise-like. This is intuitive since the principal components are more pronounced when the data has an underlying structure.

Finally, both HIPSS and Δ-HIPSS exhibit strong robustness in all cases. We see that the ROC's of HIPSS and Δ-HIPSS do not change with respect to uncertainties in noise power or the structure of the signal. Moreover, without any knowledge from field surveys, Δ-HIPSS performs only slightly worse than HIPSS. The robustness of HIPSS and Δ-HIPSS is very desirable in cognitive radio systems; additionally, compared to other protocols that require a prior field survey in determining the detection thresholds, Δ-HIPSS offers a very attractive alternative.

B. Detection Probability versus Number of Samples

In this section, we consider the relationship between the detection probability and the number of samples per observation. As shown in Section IV, the number of samples required to satisfy a pair of detection probability (P_D) and false alarm probability (P_{FA}) is a function of the SNR. Thus, we study the performance of HIPSS and Δ-HIPSS compared to the energy detector and the MME detector by fixing $P_{FA} = 0.1$ and SNR $= -15$ dB, and then plotting the detection probability versus the number of samples. Moreover, we consider two signal structures: a quadrature sinusoid and a quadrature noise-like signal. The results are shown in Fig. 6.

We make two observations; first, the MME detector does not perform well when the signal is unstructured, regardless of the number of samples. Second, the empirically obtained number of samples to satisfy a pair of false alarm and detection probabilities using a HIPSS detector is indeed twice that of using an energy detector without any noise uncertainty.

C. Detection Probability versus SNR: $\sigma_1 = \sigma_2$

In this section, we again study the performance of HIPSS compared to the energy detector and the MME detector by fixing $P_{FA} = 0.1$ and 12,000 samples per observation, and then plotting the detection probability versus SNR. We again consider both a quadrature sinusoidal signal and also a quadrature noise-like signal such that the variance of the signal is equal to the noise power multiplied by the SNR. We include the results in Fig. 7.

As in the last section, we again make two observations: first, in the presence of a noise-like signal, the MME detector behaves poorly even with a high SNR. This observation is expected based on the result from last section. Second, the empirical SNR to satisfy a pair of false alarm and detection probabilities using a HIPSS detector is 1.5 dB higher than that of using an energy detector. This is exactly the same as predicted by our analysis from Section V since the required number of samples is $O\left(\text{SNR}^{-2}\right)$.

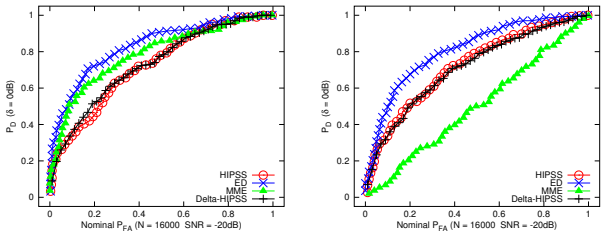

(a) ROC, noise uncertainty = 0 dB, sinusoidal signal (b) ROC, noise uncertainty = 0 dB, noise-like signal

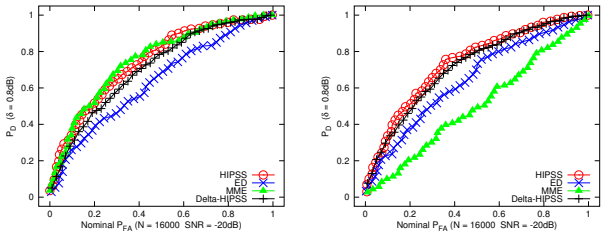

(c) ROC, noise uncertainty = 0.8 dB, sinusoidal signal (d) ROC, noise uncertainty = 0.8 dB, noise-like signal

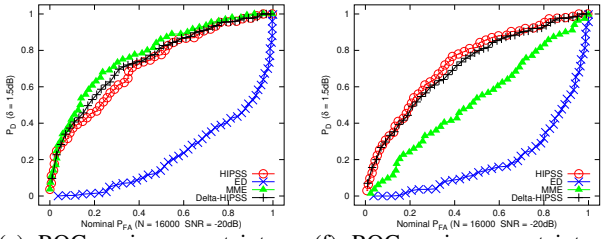

(e) ROC, noise uncertainty = 1.5 dB, sinusoidal signal (f) ROC, noise uncertainty = 1.5 dB, noise-like signal

Fig. 5: ROC's of HIPSS, sum-based energy-detector, and MME detector with either sinusoidal or AWGN signal under various noise uncertainty settings. Data generated using Octave.

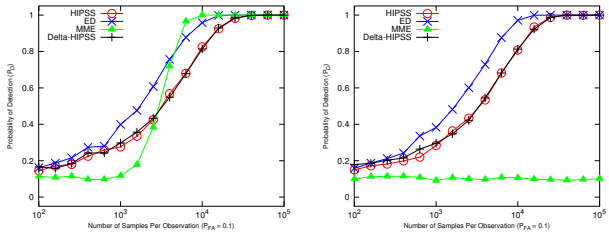

(a) P_D versus length of observations for sinusoidal signal (b) P_D versus length of observations for noise-like signal

Fig. 6: Probability of detection versus number of samples when $P_{FA} = 0.1$ and SNR $= -15$ dB. Data generated using Octave.

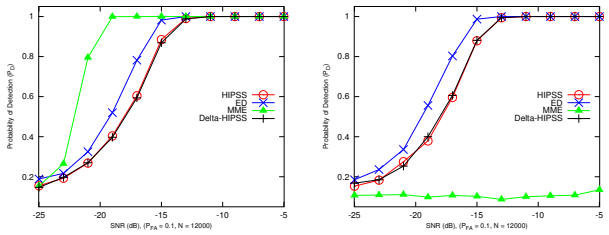

(a) P_D versus SNR (b) P_D versus SNR

Fig. 7: Probability of detection versus the signal to noise ratio when $P_{FA} = 0.1$ and each observation is 12,000 samples long. Data generated using Octave.

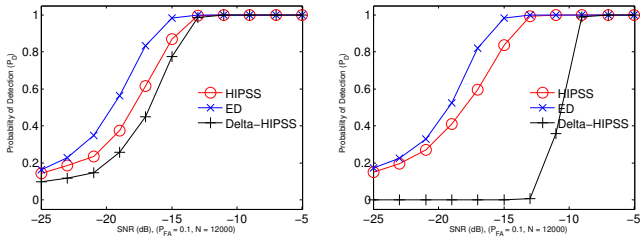

(a) P_D versus SNR, $\sigma_1^2/\sigma_2^2 = 2$ (b) P_D versus SNR, $\sigma_1^2/\sigma_2^2 = 10$

Fig. 8: Probability of detection versus the signal to noise ratio when $P_{FA} = 0.1$ and each observation is 12,000 samples long. Data generated using Octave.

D. Detection Probability versus SNR: $\sigma_1 \neq \sigma_2$

In the previous sections, we observe that when each of the two observations is corrupted by noise of same variance, the estimate of the product $\sigma_1^2\sigma_2^2$ is accurate and Δ-HIPSS provides almost identical level of performance as HIPSS. In this section, we explore the impact on the performance of Δ-HIPSS when each of the two observations is corrupted by noise with different variances. We compare the performance of Δ-HIPSS to HIPSS and the energy detector by fixing $P_{FA} = 0.1$ and taking 12,000 samples per observation.

In this section, we consider only a quadrature noise-like signal with unity power. For Δ-HIPSS and HIPSS, the variance of the signal (before being split in half) is σ_1^2 and σ_2^2 smaller than the variance of the noises added, respectively, to the first and second observations. To obtain a fair comparison, for the energy detector, we let the SNR be the ratio between the signal power and the geometric mean of the noise variances (i.e. SNR $= \frac{1}{\sigma_1\sigma_2} \leq \frac{1}{\sqrt{2K\sigma_{nn}^*}}$). We again let SNR $= -15$ dB. In Fig. 7b, we show the detection probability versus SNR when $\sigma_1^2/\sigma_2^2 = 1$; we plot the detection probability versus SNR when $\sigma_1^2/\sigma_2^2 \in \{2, 10\}$ in Fig. 8.

We observe that as the ratio σ_1^2/σ_2^2 deviates farther from 1, the performance of Δ-HIPSS degrades compared to HIPSS and the energy detector. This matches with our analysis in Section V: if the noise variances are significantly different, Δ-HIPSS would overestimate σ_{nn}^*, and decrease the detection probability.

VIII. Discussion

A. Computation Complexity of HIPSS

Even though an energy detector faces numerous challenges and drawbacks in real-life, it is by far the most popular spectrum sensing technique for one reason: *simplicity*. The attractiveness of an energy detector applies also to HIPSS since HIPSS has comparable computation complexity.

An energy detector absolute squares each sample ($2K$ multiplications: K for each of in-phase and quadrature observations), and then sums the squares ($2K - 1$ additions) for a total of $4K - 1$ floating point operations (flops). In HIPSS, the detector element-wise multiplies the in-phase (and quadrature)

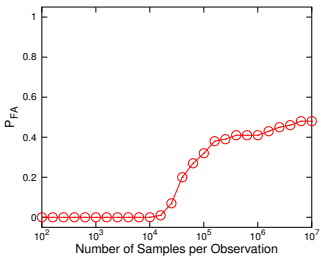

Fig. 9: False alarm probability versus the number of samples per observation. Data collected using USRP.

part of the first observation by the in-phase (and quadrature) part of the second observation ($2K$ multiplications), then sums the result ($2K-1$ additions), and finally divide the sum by K, for a total of $4K$ floating point operations.

The variance-estimation in Δ-HIPSS first subtract one observation from the other ($2K$ subtractions), then takes the absolute square of the difference ($2K$ multiplications), then sums the absolute squares ($2K-1$ additions), and finally divide by $8K^3$ (4 divisions). Together with the complexity of HIPSS, the complexity of Δ-HIPSS is $10K+3$ flops.

In Section VI, we show that HIPSS offers real-life performance similar to or better than an energy detector. Thus, for a receiver that has multiple ADCs but without a readily accessible power meter, HIPSS and Δ-HIPSS are logical alternatives to energy detection.

B. Limitations of Δ-HIPSS

While Δ-HIPSS is very robust to noise-like signals, its strength turns out to be also its weakness if misused. For example, the Sun is a particular point source of noise in the sky, thus with sufficiently many samples, Δ-HIPSS can even detect the Sun's signal (known as radio astronomy). Detecting the Sun may not be so interesting to the secondary user, for most users would wish to be able to access vacant spectrum bands on sunny days as well as rainy days.

We use our USRP in an RF-noisy laboratory to demonstrate this drawback. We set the front-end gain to 50, and collect 100 pairs of observations each 10,000,000 samples in length. We scale one observation so that both observations have the same power. We then calculate the inner product of the first 100 to 10,000,000 tuples. A signal is detected if the inner product exceeds five times the estimated maximum product of noise variances. Each detection is a false alarm, and we plot the false alarm probability versus the number of samples per observation in Fig. 9. We observe that at 10,000 samples, the false alarm rate starts increasing, and flattens at around 0.5 after collecting 1,000,000 samples.

Be it the Sun, or an appliance that is not well-shielded, the emitted noise in any particular band is likely to be low in power. Thus, when using HIPSS or Δ-HIPSS, a secondary user should be careful and collect enough samples to determine whether a primary user is around; but should also avoid being paranoid and collect too many samples, so as to avoid declaring any random noise source as band occupancy.

IX. Conclusion

In this paper, we propose HIPSS and its extension Δ-HIPSS, two light-weight spectrum sensing methods based on the Hermitian-inner-product of the observations acquired by a multiple-ADC wireless receiver. Through extensive analysis and evaluation, we show that HIPSS and Δ-HIPSS are robust and computationally efficient for spectrum sensing. In particular: 1) compared to an energy detector, by merely acquiring twice as many samples, HIPSS provides the same detection performance with comparable computational complexity, and is much more reliable in the presence of noise power uncertainties; 2) compared to a blind feature-detector, even without incurring complex computations, HIPSS and Δ-HIPSS are able to provide much superior detection in the presence of a noise-like primary signal; 3) compared to most prior spectrum sensing schemes, Δ-HIPSS is able to reach a sensing decision without necessitating any field survey beforehand.

X. Acknowledgment

We would like to thank Dr. Steven J. Franke and Dr. Tony Q. S. Quek for the very helpful discussions.

References

[1] M. A. McHenry, P. A. Tenhula, D. McCloskey, D. A. Roberson, and C. S. Hood, "Chicago spectrum occupancy measurements & analysis and a long-term studies proposal," in *Proceedings of TAPAS*, Aug. 2006.

[2] J. Mitola, III and G. Q. Maguire, Jr., "Cognitive radio: Making software radios more personal," *IEEE Personal Communications*, vol. 6, no. 4, pp. 13–18, Aug. 1999.

[3] T. Yücek and H. Arslan, "A survey of spectrum sensing algorithms for cognitive radio applications," *IEEE Communications Surveys Tutorials*, vol. 11, no. 1, pp. 116–130, 2009.

[4] J. G. Proakis and M. Salehi, *Communication Systems Engineering*, 2nd ed. McGraw-Hill, 2002, pp. 375–381.

[5] F. F. Digham, M.-S. Alouini, and M. K. Simon, "On the energy detection of unknown signals over fading channels," in *Proceedings of the IEEE International Conference on Communications*, 2003, pp. 3575–3579.

[6] D. Cabric, A. Tkachenko, and R. Brodersen, "Spectrum sensing measurements of pilot, energy, and collaborative detection," in *Proceedings of the Military Communications Conference (MILCOM)*, Oct. 2006.

[7] Y. Yuan, P. Bahl, R. Chandra, P. A. Chou, J. I. Ferrell, T. Moscibroda, S. Narlanka, and Y. Wu, "KNOWS: Cognitive radio networks over white spaces," in *Proceedings of the Second IEEE International Symposium on New Frontiers in Dynamic Spectrum Access Networks (DySPAN)*, Apr. 2007, pp. 416–427.

[8] W. A. Gardner, "Exploitation of spectral redundancy in cyclostationary signals," *IEEE Signal Processing Magazine*, vol. 8, pp. 14–36, Apr. 1991.

[9] Y. Zeng and Y.-C. Liang, "Eigenvalue-based spectrum sensing algorithms for cognitive radio," *IEEE Transactions on Communications*, vol. 57, no. 6, pp. 1784–1793, Jun. 2009.

[10] H. Sadeghi and P. Azmi, "A novel primary user detection method for multiple-antenna cognitive radio," in *Proceedings of the International Symposium on Telecommunications*, Aug. 2008, pp. 188–192.

[11] A. Taherpour, M. Nasiri-Kenari, and S. Gazor, "Multiple antenna spectrum sensing in cognitive radios," *IEEE Transactions on Wireless Communications*, vol. 9, pp. 814–823, Feb. 2010.

[12] R. Sharma and J. Wallace, "Correlation-based sensing for cognitive radio networks: Bounds and experimental assessment," *IEEE Sensors Journal*, vol. 11, no. 3, pp. 657 –666, Mar. 2011.

[13] M. S. Oude Alink, A. B. J. Kokkeler, E. A. M. Klumperink, G. J. M. Smit, and B. Nauta, "Lowering the SNR-wall for energy detection using crosscorrelation," *IEEE Transaction on Vehicular Technology*, vol. 60, no. 8, pp. 3748–3757, Oct. 2011.